Topologically Protected Quantum Coherence in a Superatom – Supplemental Material

Wei Nie,[1,2] Z. H. Peng,[3] Franco Nori,[4,5] and Yu-xi Liu[1,2,*]

[1] *Institute of Microelectronics, Tsinghua University, Beijing 100084, China*
[2] *Frontier Science Center for Quantum Information, Beijing, China*
[3] *Key Laboratory of Low-Dimensional Quantum Structures and Quantum Control of Ministry of Education, Key Laboratory for Matter Microstructure and Function of Hunan Province, Department of Physics and Synergetic Innovation Center for Quantum Effects and Applications, Hunan Normal University, Changsha 410081, China*
[4] *Theoretical Quantum Physics Laboratory, RIKEN Cluster for Pioneering Research, Wako-shi, Saitama 351-0198, Japan*
[5] *Physics Department, The University of Michigan, Ann Arbor, Michigan 48109-1040, USA*

This supplemental material provides details of the results presented in the main text.

I. 3D INTEGRATED SUPERCONDUCTING QUANTUM CIRCUITS

We consider 3D integrated superconducting quantum circuits [S1, S2] to simulate and detect many-body systems. In quantum computation, two-dimensional arrays require multi-layer wiring [S3, S4]. In Fig. S1(a), we show the 3D circuit QED with an atom array. The top layer contains a transmission line resonator and an atom array. The atoms in the array are coupled by LC resonators (not shown). The superconducting coplanar waveguides are fabricated on the bottom layer, as shown in Fig. S1(b). The atoms can be coupled to the waveguides via vertical interconnects [S1, S2]. Here, we consider that these two atoms in the same unit cells are coupled to the same waveguides. The coupling of two atoms to a waveguide is presented in Fig. S1(c). We assume that atoms A and B have the same frequency ω_0. The effective coupling and correlated decay of these two atoms are [S5, S6],

$$g_{AB}=\frac{\gamma_0}{2}\sin\Big(\frac{2\pi d_{AB}}{\lambda_0}\Big),\qquad \gamma_{AB}=\gamma_0\cos\Big(\frac{2\pi d_{AB}}{\lambda_0}\Big), \tag{S1}$$

respectively. Here, γ_0 is the decay rate of the atoms to the waveguide, $\lambda_0=2\pi c/\omega_0$, and d_{AB} is the distance between atoms A and B along the waveguide. As the positions of the atoms are properly chosen, e.g., $d_{AB}=m\lambda_0$ (m is an integer), the interaction between these two atoms can be zero, but the correlated decay of the two atoms is maximum [S6]. In Fig. S1(d), we show the atom array coupled by LC resonators. The resonator modes are represented by operators $\hat{a}_j,\hat{b}_j,\hat{c}_j,\hat{d}_j$ with $j\in[1,N-1]$.

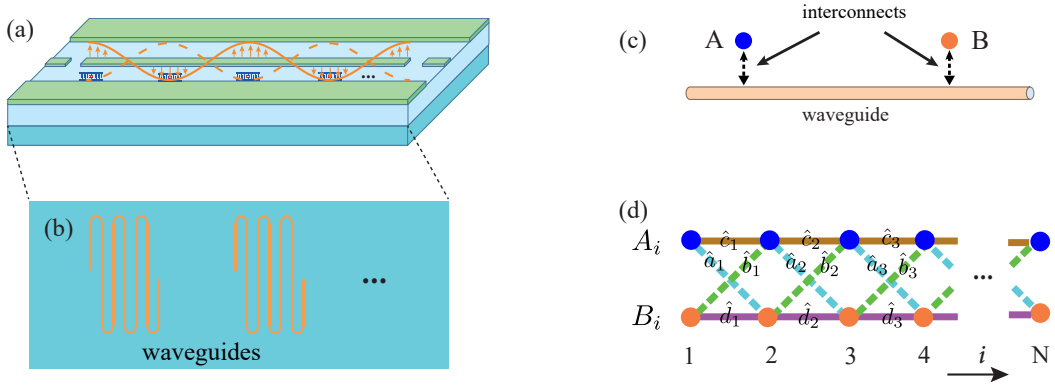

FIG. S1. (a) Schematic of 3D circuit QED with a topological atom array. The atoms in the array interact with their neighboring atoms via LC resonators, as shown in Fig.1(b) in the main text. (b) The bottom layer with superconducting coplanar waveguides. Each waveguide couples to a unit cell on the top layer. (c) The atoms A and B in a unit cell couple to a waveguide via interconnects in the middle layer. (d) Resonator-mediated atom array (see Fig.1(b) in the main text). Here the operators $\hat{\mu}_j$, with $\mu=a,b,c,d$ and $j\in[1,N-1]$, correspond to resonator modes. The index i labels the unit cell of the lattice.

* yuxiliu@mail.tsinghua.edu.cn

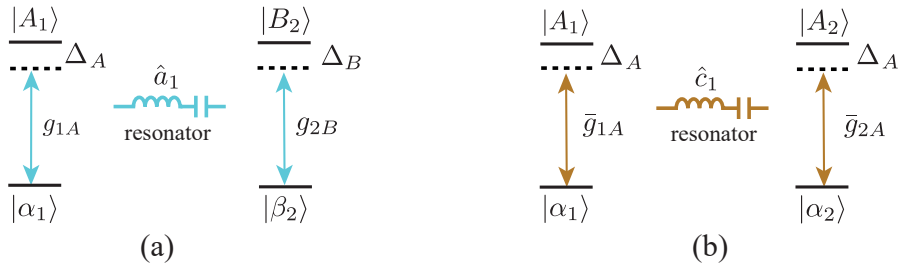

FIG. S2. Single-resonator-mediated two atoms. (a) The coupler $\hat{a}_1$ mediates the interaction between atoms A_1 and B_2. (b) The two atoms A_1 and A_2 are mediated by a resonator $\hat{c}_1$.

A. single-resonator coupled two atoms

As an example, we consider the resonator-mediated interaction between atom A and and atom B in the first and second unit cells [shown in Fig. S2(a)], respectively. The Hamiltonian is

$$H_{AB} = \omega_{a_1}\hat{a}_1^\dagger\hat{a}_1 + \omega_{1A}\sigma_{1A}^+\sigma_{1A}^- + \omega_{2B}\sigma_{2B}^+\sigma_{2B}^- - g_{1A}(\hat{a}_1^\dagger\sigma_{1A}^- + \sigma_{1A}^+\hat{a}_1) - g_{2B}(\hat{a}_1^\dagger\sigma_{2B}^- + \sigma_{2B}^+\hat{a}_1), \tag{S2}$$

with $\omega_{1A} = \omega_{2B} = \omega_0$. Here, $\hat{a}_1$ and $\hat{a}_1^\dagger$ represent the annihilation and creation operators of the LC resonator mode that couples to the A_1 and B_2 atoms. The operators for atoms A and B are $\sigma_{1A}^+ = |A_1\rangle\langle\alpha_1|$ and $\sigma_{2B}^+ = |B_2\rangle\langle\beta_2|$. We use $|\alpha_i\rangle$ and $|\beta_i\rangle$ to represent the ground states of the A and B atoms in the ith unit cell. We use $g_{i\mu}$ ($\mu = A, B$) to denote the resonator-atom couplings [see Fig. S2(a)]. In Eq. (S2), the total number of excitations is conserved. Therefore, we can rewrite the Hamiltonian in a rotating frame with $H_{\rm rot} = \omega_{a_1}(\hat{a}_1^\dagger\hat{a}_1 + \sigma_{1A}^+\sigma_{1A}^- + \sigma_{2B}^+\sigma_{2B}^-)$. The Hamiltonian becomes

$$H'_{AB} = \Delta_A\sigma_{1A}^+\sigma_{1A}^- + \Delta_B\sigma_{2B}^+\sigma_{2B}^- - g_{1A}(\hat{a}_1^\dagger\sigma_{1A}^- + \sigma_{1A}^+\hat{a}_1) - g_{2B}(\hat{a}_1^\dagger\sigma_{2B}^- + \sigma_{2B}^+\hat{a}_1). \tag{S3}$$

where $\Delta_A = \omega_{1A} - \omega_{a_1}$ and $\Delta_B = \omega_{2B} - \omega_{a_1}$. We now make a unitary transformation with

$$U = \exp[M] = \exp\left[\frac{g_{1A}}{\Delta_A}(\hat{a}_1^\dagger\sigma_{1A}^- - \sigma_{1A}^+\hat{a}_1) + \frac{g_{2B}}{\Delta_B}(\hat{a}_1^\dagger\sigma_{2B}^- - \sigma_{2B}^+\hat{a}_1)\right]. \tag{S4}$$

We obtain

$$\tilde{H}_{AB} = UH'_{AB}U^\dagger = H'_{AB} + [M, H'_{AB}] + \frac{1}{2!}[M, [M, H'_{AB}]] + \ldots \tag{S5}$$

When the detunings are large, i.e.,

$$g_{1A}, g_{2B} \ll \Delta_A, \Delta_B, \tag{S6}$$

it is reasonable to consider the effective Hamiltonian to second order in the coupling coefficients g_{1A}, g_{2B}. We can then obtain

$$\tilde{H}_{AB} = \left(\Delta_A + \frac{g_{1A}^2}{\Delta_A}\right)\sigma_{1A}^+\sigma_{1A}^- + \left(\Delta_B + \frac{g_{2B}^2}{\Delta_B}\right)\sigma_{2B}^+\sigma_{2B}^- + \frac{g_{1A}g_{2B}}{2}\left(\frac{1}{\Delta_A} + \frac{1}{\Delta_B}\right)(\sigma_{1A}^+\sigma_{2B}^- + \sigma_{2B}^+\sigma_{1A}^-). \tag{S7}$$

The terms g_{1A}^2/Δ_A and g_{2B}^2/Δ_B are the Lamb shifts for atoms A and B, respectively. The last term in the above Hamiltonian is the effective coupling between these two atoms. We call it *cross coupling*, because it couples different kinds of atoms. As shown in Fig. S1(a), the bright blue dashed lines represent cross couplings. For simplicity, we consider $g_{iA} = g_A$ and $g_{iB} = g_B$. The cross coupling is

$$t_c = \frac{g_A g_B}{2}\left(\frac{1}{\Delta_A} + \frac{1}{\Delta_B}\right). \tag{S8}$$

The couplings between the same atoms can also be implemented. These couplings are called *parallel couplings* for realizing the couplings between the same kinds of atoms. For example, the effective Hamiltonian for atoms A_1 and A_2 [as shown in Fig. S2(b)] is

$$\tilde{H}_{AA} = \left(\Delta_A + \frac{\bar{g}_{1A}^2}{\Delta_A}\right)\sigma_{1A}^+\sigma_{1A}^- + \left(\Delta_A + \frac{\bar{g}_{2A}^2}{\Delta_A}\right)\sigma_{2A}^+\sigma_{2A}^- + \frac{\bar{g}_{1A}\bar{g}_{2A}}{\Delta_A}(\sigma_{1A}^+\sigma_{2A}^- + \sigma_{2A}^+\sigma_{1A}^-). \tag{S9}$$

As we consider $\bar{g}_{iA} = \bar{g}_A$, the effective coupling between atoms A becomes

$$t_p = \frac{\bar{g}_A^2}{\Delta_A}. \tag{S10}$$

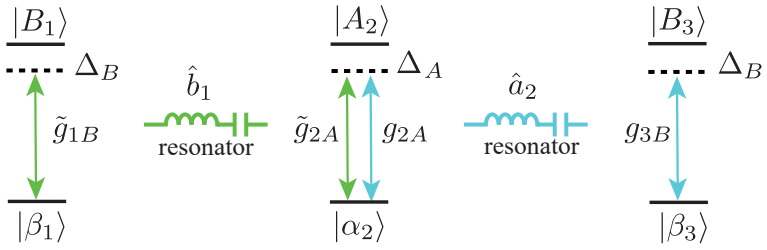

FIG. S3. Two-resonator-mediated three atoms.

B. two-resonator coupled three atoms

In our system, one atom is coupled to several atoms via different virtual-photons-exchange interactions. We now consider three atoms which are mediated by two LC resonators, as shown in Fig. S3. The corresponding Hamiltonian is

$$\begin{aligned} H_{BAB} =&\omega_{b_1}\hat{b}_1^\dagger\hat{b}_1+\omega_{a_2}\hat{a}_2^\dagger\hat{a}_2+\omega_B\sigma_{1B}^+\sigma_{1B}^-+\omega_A\sigma_{2A}^+\sigma_{2A}^-+\omega_B\sigma_{3B}^+\sigma_{3B}^- \\ &-(\tilde{g}_{1B}\hat{b}_1^\dagger\sigma_{1B}^-+\tilde{g}_{2A}\hat{b}_1^\dagger\sigma_{2A}^-+\text{H.c.})-(g_{2A}\hat{a}_2^\dagger\sigma_{2A}^-+g_{3B}\hat{a}_2^\dagger\sigma_{3B}^-+\text{H.c.}). \end{aligned} \tag{S11}$$

Here, we assume $\omega_{b_1}=\omega_{a_2}=\omega_r$. Similar to the last section, in the rotating frame, we have

$$\begin{aligned} H'_{BAB} =&\Delta_B\sigma_{1B}^+\sigma_{1B}^-+\Delta_A\sigma_{2A}^+\sigma_{2A}^-+\Delta_B\sigma_{3B}^+\sigma_{3B}^- \\ &-(\tilde{g}_{1B}\hat{b}_1^\dagger\sigma_{1B}^-+\tilde{g}_{2A}\hat{b}_1^\dagger\sigma_{2A}^-+\text{H.c.})-(g_{2A}\hat{a}_2^\dagger\sigma_{2A}^-+g_{3B}\hat{a}_2^\dagger\sigma_{3B}^-+\text{H.c.}), \end{aligned} \tag{S12}$$

where $\Delta_B=\omega_B-\omega_r$ and $\Delta_A=\omega_A-\omega_r$. For simplicity, the above Hamiltonian can be expressed as

$$H'_{BAB}=H_1+H_2+H_3+H_{12}+H_{23}, \tag{S13}$$

where $H_{1,2,3}$ are the Hamiltonians for individual atoms. Here, H_{12} and H_{23} are interactions mediated by LC resonators. We make a unitary transformation $\tilde{U}=\exp[\tilde{M}]$, with $\tilde{M}=M_1+M_2$. Here, M_1 and M_2 are given by

$$\begin{aligned} M_1&=\frac{\tilde{g}_{1B}}{\Delta_B}(\hat{b}_1^\dagger\sigma_{1B}^--\sigma_{1B}^+\hat{b}_1)+\frac{\tilde{g}_{2A}}{\Delta_A}(\hat{b}_1^\dagger\sigma_{2A}^--\sigma_{2A}^+\hat{b}_1), \\ M_2&=\frac{g_{2A}}{\Delta_A}(\hat{a}_2^\dagger\sigma_{2A}^--\sigma_{2A}^+\hat{a}_2)+\frac{g_{3B}}{\Delta_B}(\hat{a}_2^\dagger\sigma_{3B}^--\sigma_{3B}^+\hat{a}_2). \end{aligned} \tag{S14}$$

Then,

$$\tilde{U}H'_{BAB}\tilde{U}^\dagger=H'_{BAB}+[\tilde{M},H'_{BAB}]+\frac{1}{2!}[\tilde{M},[\tilde{M},H'_{BAB}]]+\ldots, \tag{S15}$$

with $[\tilde{M},H'_{BAB}]=[M_1,H'_{BAB}]+[M_2,H'_{BAB}]$. We first consider the term $[M_1,H'_{BAB}]$,

$$[M_1,H'_{BAB}]=[M_1,H_1+H_2+H_{12}]+[M_1,H_{23}]. \tag{S16}$$

We now look at the second term on the right-hand side of the above expression,

$$\begin{aligned} [M_1,H_{23}]&=\Big[\frac{\tilde{g}_{2A}}{\Delta_A}(\hat{b}_1^\dagger\sigma_{2A}^--\sigma_{2A}^+\hat{b}_1),-g_{2A}(\hat{a}_2^\dagger\sigma_{2A}^-+\sigma_{2A}^+\hat{a}_2)\Big] \\ &=-\frac{\tilde{g}_{2A}g_{2A}}{\Delta_A}(\hat{b}_1^\dagger\hat{a}_2+\hat{a}_2^\dagger\hat{b}_1)(|\alpha_2\rangle\langle\alpha_2|-|A_2\rangle\langle A_2|). \end{aligned} \tag{S17}$$

In our system, the couplers are set to be vacuum states. The real photon exchange can be ignored. Therefore, $[M_1,H_{23}]=0$. So,

$$[\tilde{M},H'_{BAB}]=[M_1,H_1+H_2+H_{12}]+[M_2,H_2+H_3+H_{23}]. \tag{S18}$$

Similarly,

$$\begin{aligned} [\tilde{M},[\tilde{M},H'_{BAB}]]=&\quad[M_1,[M_1,H_1+H_2+H_{12}]]+[M_2,[M_2,H_2+H_3+H_{23}]] \\ &+[M_2,[M_1,H_1+H_2+H_{12}]]+[M_1,[M_2,H_2+H_3+H_{23}]]. \end{aligned} \tag{S19}$$

To second order in g, we have

$$[M_2,[M_1,H_1+H_2+H_{12}]]=0, \tag{S20}$$

and

$$[M_1,[M_2,H_2+H_3+H_{23}]]=0. \tag{S21}$$

Hence,

$$[\tilde{M},[\tilde{M},H'_{BAB}]]=[M_1,[M_1,H_1+H_2+H_{12}]]+[M_2,[M_2,H_2+H_3+H_{23}]]. \tag{S22}$$

Therefore,

$$\begin{aligned}\tilde{H}_{BAB}&=\tilde{U}H'_{BAB}\tilde{U}^\dagger\\&=\Big(\Delta_B+\frac{\tilde{g}_{1B}^2}{\Delta_B}\Big)\sigma_{1B}^+\sigma_{1B}^-+\Big(\Delta_A+\frac{\tilde{g}_{2A}^2+g_{2A}^2}{\Delta_A}\Big)\sigma_{2A}^+\sigma_{2A}^-+\Big(\Delta_B+\frac{g_{3B}^2}{\Delta_B}\Big)\sigma_{3B}^+\sigma_{3B}^-\\&\quad+\frac{\tilde{g}_{1B}\tilde{g}_{2A}}{2}\Big(\frac{1}{\Delta_A}+\frac{1}{\Delta_B}\Big)(\sigma_{1B}^+\sigma_{2A}^-+\sigma_{2A}^+\sigma_{1B}^-)+\frac{g_{2A}g_{3B}}{2}\Big(\frac{1}{\Delta_A}+\frac{1}{\Delta_B}\Big)(\sigma_{2A}^+\sigma_{3B}^-+\sigma_{3B}^+\sigma_{2A}^-).\end{aligned} \tag{S23}$$

This effective Hamiltonian shows that the chain-like coupling scheme, as shown in Fig. S3, does not lead to long-range couplings between atoms. By assuming $\tilde{g}_{1B}=g_{3B}=g_B$ and $\tilde{g}_{2A}=-g_{2A}=-g_A$, Eq. (S23) can be written as

$$\begin{aligned}\tilde{H}_{BAB}=&\Big(\Delta_B+\frac{g_B^2}{\Delta_B}\Big)\sigma_{1B}^+\sigma_{1B}^-+\Big(\Delta_A+2\frac{g_A^2}{\Delta_A}\Big)\sigma_{2A}^+\sigma_{2A}^-+\Big(\Delta_B+\frac{g_B^2}{\Delta_B}\Big)\sigma_{3B}^+\sigma_{3B}^-\\&+(-t_c\sigma_{1B}^+\sigma_{2A}^-+t_c\sigma_{2A}^+\sigma_{3B}^-+\text{H.c.}).\end{aligned} \tag{S24}$$

C. boundary conditions

Using the periodic boundary conditions, the translational invariance makes the Lamb shifts for the same kinds of atoms to be equal. We denote the energy splitting between atoms A and B to be 2δ. Then, the effective Hamiltonian becomes

$$\tilde{H}=\sum_{i=1}^{N}\Big[\frac{\delta}{2}(\sigma_{iA}^+\sigma_{iA}^--\sigma_{iB}^+\sigma_{iB}^-)+t_p(\sigma_{iA}^+\sigma_{i+1A}^--\sigma_{iB}^+\sigma_{i+1B}^-)-t_c(\sigma_{iA}^+\sigma_{i+1B}^--\sigma_{iB}^+\sigma_{i+1A}^-)\Big]+\text{H.c.}, \tag{S25}$$

with $\sigma_{N+1\mu}^\pm=\sigma_{1\mu}^\pm$ ($\mu=A,B$). In Eq. (S25), the effective couplings have been simplified. The topological property is analysed in the main text. Using open boundary conditions, the atoms of unit cells at the boundaries have different Lamb shifts compared to atoms in other unit cells. However, we can couple vacuum resonators or cavities to these boundary atoms to generate additional Lamb shifts, such that all the atoms of the same kind have the same energy.

II. TOPOLOGICAL SUPERATOM

The single-excitation subspace is well-separated from multiple-excitation subspaces, as shown in Fig. S4(a). In our model with superconducting quantum circuits, t_c and t_p are tens of MHz, $\tilde{\omega}_0$ is several GHz. We denote $|\mathcal{A}_i\rangle=\sigma_{iA}^+|G\rangle$ and $|\mathcal{B}_i\rangle=\sigma_{iB}^+|G\rangle$ with $|G\rangle=|\alpha_1\beta_1\alpha_2\beta_2\cdots\rangle$ being the ground state of the atom array. Then we have

$$\langle\mathcal{A}_i|\sigma_{iA}^+\sigma_{i+1A}^-|\mathcal{A}_{i+1}\rangle=\langle G|G\rangle=1, \tag{S26}$$

and similarly $\langle\mathcal{B}_i|\sigma_{iB}^+\sigma_{i+1B}^-|\mathcal{B}_{i+1}\rangle=1$, $\langle\mathcal{A}_i|\sigma_{iA}^+\sigma_{i+1B}^-|\mathcal{B}_{i+1}\rangle=1$, $\langle\mathcal{B}_i|\sigma_{iB}^+\sigma_{i+1A}^-|\mathcal{A}_{i+1}\rangle=1$. Therefore, the Hamiltonian Eq.(3) in the main text can be written in the single-excitation subspace $\{|\mathcal{A}_i\rangle,|\mathcal{B}_i\rangle\}$ as

$$\bar{H}=\sum_{i=1}^{N}\Big[\frac{\delta}{2}(|\mathcal{A}_i\rangle\langle\mathcal{A}_i|-|\mathcal{B}_i\rangle\langle\mathcal{B}_i|)+t_p(|\mathcal{A}_i\rangle\langle\mathcal{A}_{i+1}|-|\mathcal{B}_i\rangle\langle\mathcal{B}_{i+1}|)-t_c(|\mathcal{A}_i\rangle\langle\mathcal{B}_{i+1}|-|\mathcal{B}_i\rangle\langle\mathcal{A}_{i+1}|)\Big]+\text{H.c.}. \tag{S27}$$

In crystal momentum space, the Hamiltonian becomes $\bar{H}(k)=\sum_k\Psi_k^\dagger h(k)\Psi_k$, with $\Psi_k^\dagger=(|\mathcal{A}_k\rangle,|\mathcal{B}_k\rangle)$, and

$$h(k)=d_y(k)\sigma_y+d_z(k)\sigma_z, \tag{S28}$$

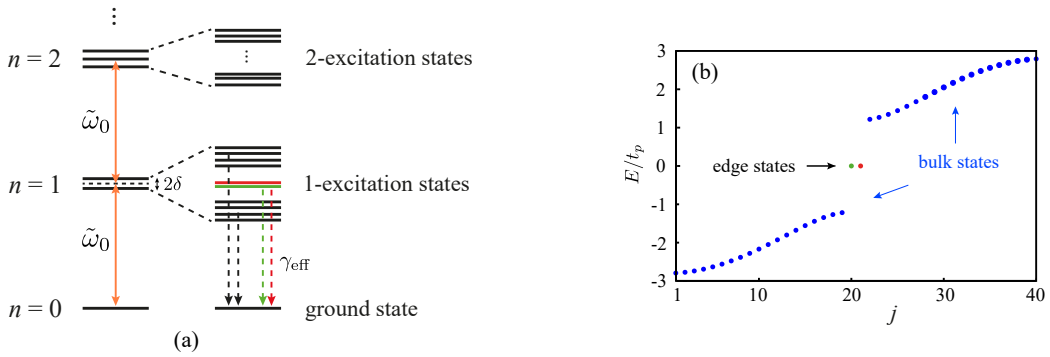

FIG. S4. Topological superatom. (a) Energy levels for subspaces with different excitations. The energy levels on the left side are produced when t_c and t_p are zero. Here $\tilde{\omega}_0$ represents the middle frequency of atoms A and B. On the right side, finite t_c and t_p split the energy degeneracies in single-excitation and multiple-excitation subspaces. Due to $t_c, t_p \ll \tilde{\omega}_0$, the single-excitation subspace is separated from the two-excitation subspace. (b) Large gaps between edge states and bulk states in the single-excitation subspace of the atom array. Here j labels the eigenstates of the atom array in the single-excitation subspace and the number of unit cells is $N = 20$.

where $d_y(k) = 2t_c \sin k$ and $d_z(k) = \delta + 2t_p \cos k$.

Edge states are topologically protected quantum many-body states. They are able to encode quantum information and can be used as topological qubits. Recently, the study of Majorana zero modes has advanced considerably. Topological quantum computation can be potentially implemented with Majorana fermions. There are theoretical proposals suggesting that photon-electron interactions could be used to control Majorana fermions. However, the photon-electron interactions are not easy to control, compared to light-atom interactions. Especially, in some artificial atoms, e.g., superconducting quantum circuits, one can optically manipulate quantum states of atoms with high accuracy.

The 1D atom array studied here has a complex energy spectrum. In its topological phase, as shown in Fig. S4(b), bulk states exhibit a smooth spectrum with very small gaps among the bulk states. This makes it difficult to address specific quantum many-body states. However, there are large gaps between the two $E = 0$ edge states and bulk states. This provides a strong nonlinearity to control the edge states. In quantum systems, the nonlinearity of energy levels is critical for qubits or qutrits, where quantum information can be encoded. Due to the large gaps between edge states and bulk states, the topological superatom with a ground state and two edge states can be used to characterize the atom array. We can exploit the properties of edge states, i.e., topology-protected spin polarization and boundary localization, to implement the interaction between light and the topological superatom. Benefiting from the atom-light couplings, which are studied in many quantum optical systems, the topological superatom could be easily addressed.

A. Edge states in the single-excitation subspace

The atom array mediated by couplers is shown to have topological structure in crystal momentum space. From the edge-bulk correspondence, edge states can be generated in the topological phase with open boundary conditions. Different from normal many-body states, edge states have peculiar properties that can be employed for topological quantum state engineering. Therefore, we better analyze the wavefunctions of edge states. In the single-excitation subspace, the Hamiltonian can be written as [S7, S8],

$$\bar{H} = \sum_{i=1}^{N} \mathcal{M}\Psi_i^\dagger \Psi_i + \mathcal{T}^\dagger \Psi_{i+1}^\dagger \Psi_i + \mathcal{T}\Psi_i^\dagger \Psi_{i+1}, \tag{S29}$$

with

$$\mathcal{M} = \delta\sigma_z, \qquad \mathcal{T} = t_p\sigma_z + it_c\sigma_y.$$

We now make an ansatz for the edge state $\psi = \sum_n \lambda^n \phi$, where ϕ is a 2 component spinor. Therefore,

$$\bar{H}\psi = E\psi. \tag{S30}$$

From the above equation, we can have

$$(\mathcal{M} + \lambda\mathcal{T}^\dagger + \lambda^{-1}\mathcal{T})\phi = E\phi. \tag{S31}$$

This can be written as

$$[\delta\sigma_z + \lambda(t_p\sigma_z - it_c\sigma_y) + \lambda^{-1}(t_p\sigma_z + it_c\sigma_y)]\phi = E\phi. \tag{S32}$$

The edge states are solutions with $E = 0$, i.e.,

$$[\delta\sigma_z + \lambda(t_p\sigma_z - it_c\sigma_y) + \lambda^{-1}(t_p\sigma_z + it_c\sigma_y)]\phi = 0. \tag{S33}$$

Multiplying σ_z from the left-hand side, one obtains

$$[\delta + \lambda(t_p - t_c\sigma_x) + \lambda^{-1}(t_p + t_c\sigma_x)]\phi = 0. \tag{S34}$$

We can obtain the eigenstates $\phi_\pm$ via

$$\sigma_x\phi_\pm = \pm\phi_\pm. \tag{S35}$$

From Eq. (S34), we can have $\delta + \lambda(t_p - t_c) - \lambda^{-1}(-t_p - t_c) = 0$, which is a quadratic equation for λ. It can be solved with solutions,

$$\lambda_{+,1} = \frac{\delta + \sqrt{\delta^2 + 4(t_c^2 - t_p^2)}}{2(t_c - t_p)}, \qquad \lambda_{+,2} = \frac{\delta - \sqrt{\delta^2 + 4(t_c^2 - t_p^2)}}{2(t_c - t_p)}, \tag{S36}$$

for ϕ_+, and

$$\lambda_{-,1} = \frac{\delta + \sqrt{\delta^2 + 4(t_c^2 - t_p^2)}}{2(-t_c - t_p)}, \qquad \lambda_{-,2} = \frac{\delta - \sqrt{\delta^2 + 4(t_c^2 - t_p^2)}}{2(-t_c - t_p)}. \tag{S37}$$

for ϕ_-. The values of $\lambda_{\pm,1/2}$ determine the wavefunctions of the edges states. From Eq. (S36) and Eq. (S37), we can find that $1/\lambda_{+,1} = \lambda_{-,2}$ and $1/\lambda_{+,2} = \lambda_{-,1}$. So, there are two cases that lead to different edge states in the system.

Case (1): If $|\lambda_{+,1}| < 1$ and $|\lambda_{+,2}| < 1$, the edge state of the left boundary is polarized along ϕ_+. The component of the wavefunction in the ith unit cell is

$$\psi_L(i) = \left[c_1(\lambda_{+,1})^i + c_2(\lambda_{+,2})^i\right]\phi_+^{(i)}. \tag{S38}$$

The open boundary condition requires the amplitude of $\psi_L(0)$ to be zero, which gives $c_1 = -c_2$. Therefore, the left edge state is

$$\psi_L = \frac{1}{\sqrt{\mathcal{N}_L^+}}\sum_i \left[(\lambda_{+,1})^i - (\lambda_{+,2})^i\right]\phi_+^{(i)}, \tag{S39}$$

where $\mathcal{N}_L^+$ is the normalization factor. Similarly, the right edge state with open boundary condition is

$$\psi_R = \frac{1}{\sqrt{\mathcal{N}_R^-}}\left[(\lambda_{+,1})^{N+1-i} - (\lambda_{+,2})^{N+1-i}\right]\phi_-^{(i)}. \tag{S40}$$

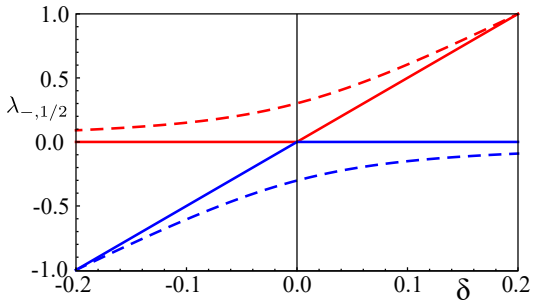

FIG. S5. The eigenvalue λ of ϕ_- (see Eq. (S37)) versus δ, with $t_p = -0.1$. The red-solid and red-dashed curves represent $\lambda_{-,1}$ with different values of t_c: -0.1 and -0.12, respectively. Similarly, the blue-solid and blue-dashed curves show $\lambda_{-,2}$ for $t_c = -0.1$ and $t_c = -0.12$, respectively. The effective energy difference between the two excited states $|A_i\rangle$ and $|B_i\rangle$ of the ith atom is 2δ.

Case (2): If $|\lambda_{+,1}| > 1$ and $|\lambda_{+,2}| > 1$, the edge state of the left boundary is polarized along ϕ_-, because of $1/\lambda_{+,1} = \lambda_{-,2}$ and $1/\lambda_{+,2} = \lambda_{-,1}$. The wavefunctions for the left and right edge states are

$$\psi_L = \frac{1}{\sqrt{\mathcal{N}_L^-}} \sum_i \left[(\lambda_{-,1})^i - (\lambda_{-,2})^i\right] \phi_-^{(i)}, \tag{S41}$$

and

$$\psi_R = \frac{1}{\sqrt{\mathcal{N}_R^+}} \sum_i \left[(\lambda_{-,1})^{N+1-i} - (\lambda_{-,2})^{N+1-i}\right] \phi_+^{(i)}. \tag{S42}$$

The values of $\lambda_{\pm,1/2}$, which are determined by the system parameters, affect the form of the edge states. In Fig. S5, we show $\lambda_{-,1/2}$ for two cases, i.e., $|t_c| = |t_p|$ and $|t_c| \neq |t_p|$ in the topological phase ($-2|t_p| < \delta < 2|t_p|$). As $|t_c| = |t_p|$, only one parameter, $\lambda_{-,1}$ or $\lambda_{-,2}$ is nonzero. However, in the case of $|t_c| \neq |t_p|$, both $\lambda_{-,1}$ and $\lambda_{-,2}$ are nonzero. This two different forms of edge states have distinctive features in the finite-size effects of the edge states, as we show in the main text.

The edge states shown above, i.e., Eqs. (S39)-(S42), describe long lattices, as shown in Fig. S6(a). For short lattices, the edge states are not separated, but hybridize with each other, as shown in Fig. S6(b). The hybridized edge states may have interesting observable effects. The hybridization leads to splitting between edge states (see Fig. S6(c)). As shown in Fig. S6(d), the hybridized edge states can be written as $\psi_\pm = \frac{1}{\sqrt{2}}(\psi_L \pm \psi_R)$, where ψ_L and ψ_R are the left and right localized edge states, respectively. We consider left edge state to be the initial state, i.e., $\psi_0 = \frac{1}{\sqrt{2}}(\psi_+ + \psi_-)$. The evolution of the system is

$$\begin{aligned}
\psi(t) &= \frac{1}{\sqrt{2}} e^{-i\tilde{H}t/\hbar}(\psi_+ + \psi_-) \\
&= \frac{1}{\sqrt{2}} e^{-i\tilde{\omega}_0 t}(e^{-i\Delta_s t}\psi_+ \ + e^{i\Delta_s t}\psi_-) \\
&= e^{-i\tilde{\omega}_0 t}\Big[\frac{1}{\sqrt{2}}\cos(\Delta_s t)(\psi_+ + \psi_-) - i\frac{1}{\sqrt{2}}\sin(\Delta_s t)(\psi_+ - \psi_-)\Big] \\
&= e^{-i\tilde{\omega}_0 t}[\cos(\Delta_s t)\psi_L - i\sin(\Delta_s t)\psi_R],
\end{aligned} \tag{S43}$$

where $\tilde{\omega}_0$ is the middle frequency of two edge states, and Δ_s represents the splitting between them. When $\Delta_s \approx 0$, the excitation localizes to the left edge of the atom array. Otherwise, the excitation oscillates between the left-edge

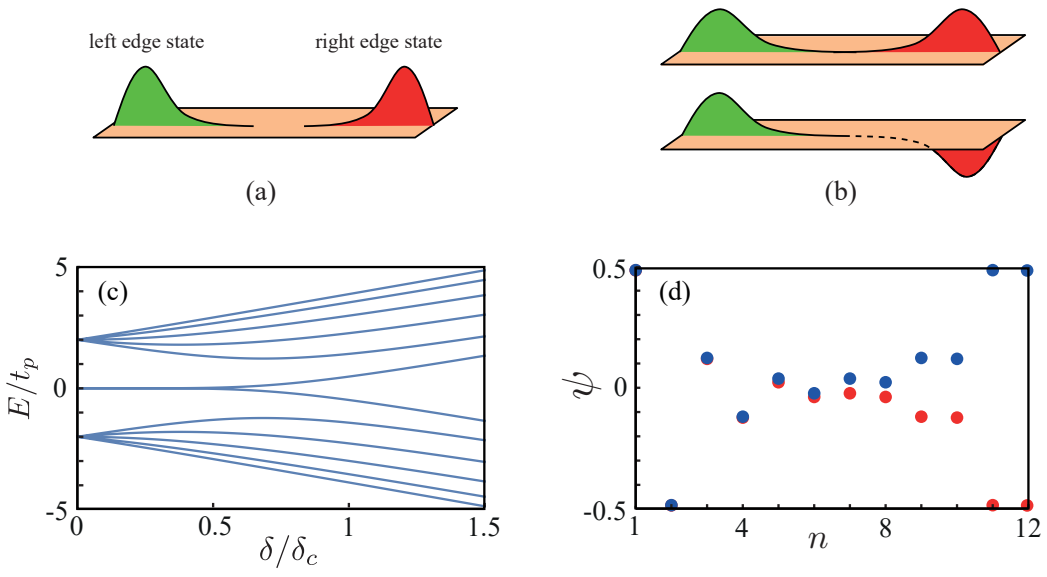

FIG. S6. (a) The left and right edge states are well separated in large arrays. (b) Edge states are hybridized due to finite size of the atom array. (c) Energy spectrum of the atom array with $N = 6$ unit cells. (d) Wavefunction of hybridized edge states for $\delta/\delta_c = 0.25$. Here n labels the positions of atoms in the array, i.e., odd (even) number of n corresponds to $|\mathcal{A}_{\frac{n+1}{2}}\rangle$ ($|\mathcal{B}_{\frac{n}{2}}\rangle$).

and right-edge atoms. This oscillatory behavior shows the interaction between edge states. Since the atoms at left and right edges are respectively subradiant and superradiant, the excitation mainly relaxes from the right edge. And from the revival of the excitation, we can estimate the decay rate of the superradiant (right) edge state. For the case $\delta/\delta_c = 0.25$, the value of Δ_s becomes $4.6\times10^{-5}\kappa$. Because of $\Delta_s \ll \gamma$, the edge states are localized during the lifetime of single atoms. However, when Δ_s becomes large ($\Delta_s \approx \gamma$), the population dynamics of the subradiant edge state can be used to measure the coupling strength of the edge states.

B. Driving a topological superatom in a cavity

In our one-dimensional topological array with V-shaped effective three-level atoms, the edge states are produced in the excited state. Moreover, thanks to symmetry protection, there are many features unique to edge states, i.e., spin polarization, boundary localization, and large energy gaps to bulk states. These properties make it feasible to optically manipulate edge states. The coupling between ground and excited edge states can be realized by choosing appropriate cavity-atom coupling parameters, such that the edge states are efficiently populated. For example, in superconducting quantum circuits, the couplings between artificial atoms and cavity can be controlled. Therefore, the topological superatom can be controlled. Here, we consider the low-excitation limit, i.e., $\langle\sigma_{i\alpha}^{+}\sigma_{i\alpha}^{-}\rangle \approx 0$, with $\alpha = A, B$. The master equation of the cavity-driving atom array is

$$\dot{\rho} = i[\rho, H_{\rm tot}] + \mathcal{L}_a[\rho] + \mathcal{L}_c[\rho], \tag{S44}$$

with total Hamiltonian $H_{\rm tot} = \tilde{H} + H_c + H_I$. Here, $\tilde{H}$ represents the coupler-mediated atom array, H_c is the Hamiltonian of the cavity, and H_I is the cavity-atom interaction. The dissipation terms for the atom array and cavity are

$$\mathcal{L}_a[\rho] = \sum_{i,\mu,\nu}\gamma_{\mu\nu}(2\sigma_{i\mu}^{-}\rho\sigma_{i\nu}^{+} - \sigma_{i\mu}^{+}\sigma_{i\nu}^{-}\rho - \rho\sigma_{i\mu}^{+}\sigma_{i\nu}^{-}), \tag{S45}$$

and

$$\mathcal{L}_c[\rho] = \kappa(2\hat{f}\rho\hat{f}^{\dagger} - \hat{f}^{\dagger}\hat{f}\rho - \rho\hat{f}^{\dagger}\hat{f}), \tag{S46}$$

respectively. From the master equation, we obtain the equations

$$\langle\frac{d}{dt}\hat{f}\rangle = -(\kappa + i\Delta_c)\langle\hat{f}\rangle - i\boldsymbol{\Xi}^{\rm T}\langle\boldsymbol{\sigma}\rangle + \eta, \tag{S47}$$

$$\langle\frac{d}{dt}\boldsymbol{\sigma}\rangle = -i(\boldsymbol{\Delta} + \boldsymbol{D} - i\boldsymbol{\Gamma})\langle\boldsymbol{\sigma}\rangle - i\boldsymbol{\Xi}\langle\hat{f}\rangle, \tag{S48}$$

with $\boldsymbol{\Xi} = (\xi_{1A}, \xi_{1B}, \xi_{2A}, \xi_{2B}, \cdots)$, $\langle\boldsymbol{\sigma}\rangle = (\langle\sigma_{1A}^{-}\rangle, \langle\sigma_{1B}^{-}\rangle, \langle\sigma_{2A}^{-}\rangle, \langle\sigma_{2B}^{-}\rangle, \cdots)^{\rm T}$, $\boldsymbol{\Delta} = {\rm Diag}(\delta, -\delta, \delta, -\delta, \cdots)$,

$$\boldsymbol{\Gamma} = \begin{pmatrix} \gamma_{1A} & \gamma_{1AB} & 0 & 0 & 0 \\ \gamma_{1AB} & \gamma_{1B} & 0 & 0 & 0 \\ 0 & 0 & \gamma_{2A} & \gamma_{2AB} & 0 \\ 0 & 0 & \gamma_{2AB} & \gamma_{2B} & 0 \\ 0 & 0 & 0 & 0 & \ddots \end{pmatrix}, \tag{S49}$$

and

$$\boldsymbol{D} = \begin{pmatrix} 0 & R & 0 & 0 \\ R^T & 0 & R & 0 \\ 0 & R^T & 0 & \ddots \\ 0 & 0 & \ddots & \ddots \end{pmatrix}, \tag{S50}$$

where

$$R = \begin{pmatrix} t_p & -t_c \\ t_c & -t_p \end{pmatrix}.$$

Here, $\xi_{i\alpha}$ are the coupling coefficients between the atoms and cavity. The steady cavity field can be solved by assuming $\langle \frac{d}{dt}\hat{f}\rangle = 0$ and $\langle \frac{d}{dt}\boldsymbol{\sigma}\rangle = 0$. Then, we can obtain the transmission

$$T = |t|^2 = \Big|\frac{\kappa}{\kappa + i\Delta_c - i\chi}\Big|^2, \tag{S51}$$

with

$$t = \kappa\langle\hat{f}\rangle/\eta \tag{S52}$$

and susceptibility

$$\chi = \boldsymbol{\Xi}^{\intercal}(\Delta + \boldsymbol{D} - i\boldsymbol{\Gamma})^{-1}\boldsymbol{\Xi}. \tag{S53}$$

When a quantum many-body state is driven by the cavity field, one can probe its optical response via its photon transmission. The susceptibility captures the central property of the cavity-driving many-body system. From the susceptibility, we can obtain the effective decay rate of the superatom,

$$\gamma_{\text{eff}} = -\text{Im}\Big[\frac{\boldsymbol{\Xi}^{\intercal}\boldsymbol{\Xi}}{\chi}\Big]. \tag{S54}$$

In particular, the edge states in the single-excitation subspace have zero energy, which makes $\text{Re}[\chi]$ vanishing. When the edge state is resonantly driven, the transmission can be expressed by the effective decay

$$T_{\text{res}} = \frac{\kappa^2}{(\kappa + \text{Im}[\chi])^2}. \tag{S55}$$

The invariance of $\text{Im}[\chi]$ for edge states indicates the topologically protected quantum coherence. As shown in Fig. 3(b), the bulk states in the non-topological phase also have constant $\text{Im}[\chi]$ when δ is large. This represents that the decay rates of bulk states have an upper bound γ. In the main text, we consider that the cavity has low decay rate κ, i.e., $\kappa = 0.1\gamma$. The cavity decay κ plays important role in the transmission of edge states. In Fig. S7(a), we consider a large cavity decay. The left edge state has clear signal as γ_{AB} increases. However, the transmission for

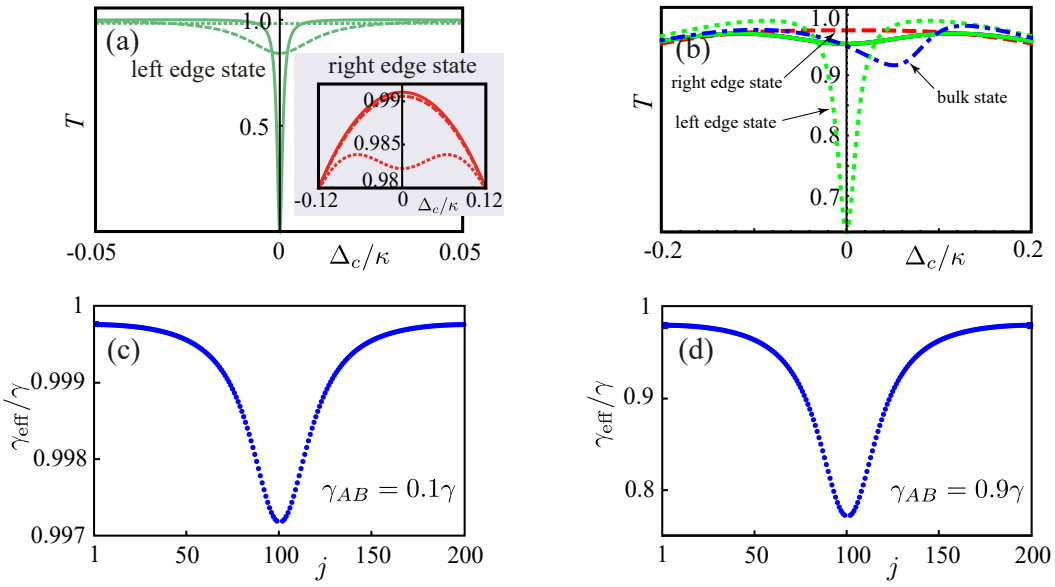

FIG. S7. (a) Transmission spectra of the left and right (the inset) edge states. Here, $\Delta_c = \omega_{\text{cavity}} - \omega_{\text{drive}}$ and $\delta/\delta_c = 0.6$. Dotted, dashed, and solid lines correspond to $\gamma_{AB}/\gamma = 0, 0.9, 1$, respectively. (b) Transmission spectra of the two edge states and one bulk state. The red-dashed(-solid), green-dotted(-solid), and blue-dot-dashed(-solid) curves are the transmissions for edge states and bulk state, with $\gamma_{AB}/\gamma = 0.9$ ($\gamma_{AB}/\gamma = 0$), $\delta/\delta_c = 0.65$. (c,d) Effective decays of bulk states for $\gamma_{AB} = 0.1\gamma$ and $\gamma_{AB} = 0.9\gamma$, respectively, with $\delta/\delta_c = 0.6$. The horizontal axis j represents bulk states from lowest energy to highest energy states (edge states with $j = 100$ and $j = 101$ are not shown). Other parameters for these figures are $N = 100, t_c = t_p, \kappa = 10\gamma$.

right edge state is not changed so much. In Fig. S7(b), the transmission spectra for two edge states and one bulk state are compared. When γ_{AB} is zero, the transmissions for edge and bulk states are the same. When γ_{AB} is nonzero, the spectrum is found to be asymmetric for bulk state, but symmetric for edge states.

As shown in the main text, the effective decay rates for bulk states and edge states are equal to γ for $\gamma_{AB} = 0$. However, nonzero correlated decay γ_{AB} makes the bulk states to be subradiant. In Figs. S7(c) and S7(d), we show the effective decays for bulk states with different values of γ_{AB}. The x axis denotes the index of the bulk states, from lowest energy to the largest (the edge states for $n = N, N+1$ in the middle are not shown). It can be seen that the effective decays for bulk states are symmetric. Moreover, the bulk states closer to edge states are more subradiant. For large correlated decay γ_{AB}, the bulk states have very different coherence properties compared with edge states; the symmetric edge state is superradiant, and the anti-symmetric edge state is very subradiant. The coherence differences between edge states and bulk states lead to distinctive collective behavior of edge atoms and bulk atoms.

III. EFFECTS OF SYMMETRY BREAKING AND DISORDERS

The waveguides mediate the correlated decays between atoms in unit cells. As shown in Eq. (S1) and Fig. S1(c), when the separation between two atoms along the waveguide coupling them is $2\pi mc/\omega_0$ (m is an integer number), the interaction between these two atoms becomes zero. In experiments, there could be imperfections, such that the separation between two atoms along the waveguide is not exactly $2\pi mc/\omega_0$. If these interactions are homogeneous, i.e., the interactions between atoms in the same unit cells are g_{AB}, the Hamiltonian of the system becomes

$$\begin{aligned}\tilde{H}' = &\sum_{i=1}^{N} \delta(\sigma_{iA}^{+}\sigma_{iA}^{-} - \sigma_{iB}^{+}\sigma_{iB}^{-}) + g_{AB}(\sigma_{iA}^{+}\sigma_{iB}^{-} + \sigma_{iB}^{+}\sigma_{iA}^{-}) \\ &+ \sum_{i=1}^{N-1} \Big[t_p(\sigma_{iA}^{+}\sigma_{i+1A}^{-} - \sigma_{iB}^{+}\sigma_{i+1B}^{-}) - t_c(\sigma_{iA}^{+}\sigma_{i+1B}^{-} - \sigma_{iB}^{+}\sigma_{i+1A}^{-}) + \text{H.c.} \Big]. \end{aligned} \tag{S56}$$

In the crystal momentum space, the Hamiltonian is $\bar{H}'(k) = \sum_k \Psi_k^{\dagger} h'(k) \Psi_k$, with

$$h'(k) = g_{AB}\sigma_x + d_y(k)\sigma_y + d_z(k)\sigma_z. \tag{S57}$$

Apparently, the interactions between atoms in the same unit cells break the chiral symmetry. Accordingly, the energy degeneracy between left- and right-edge states is shifted, as shown in Fig. S8(a). However, the edge polarizations

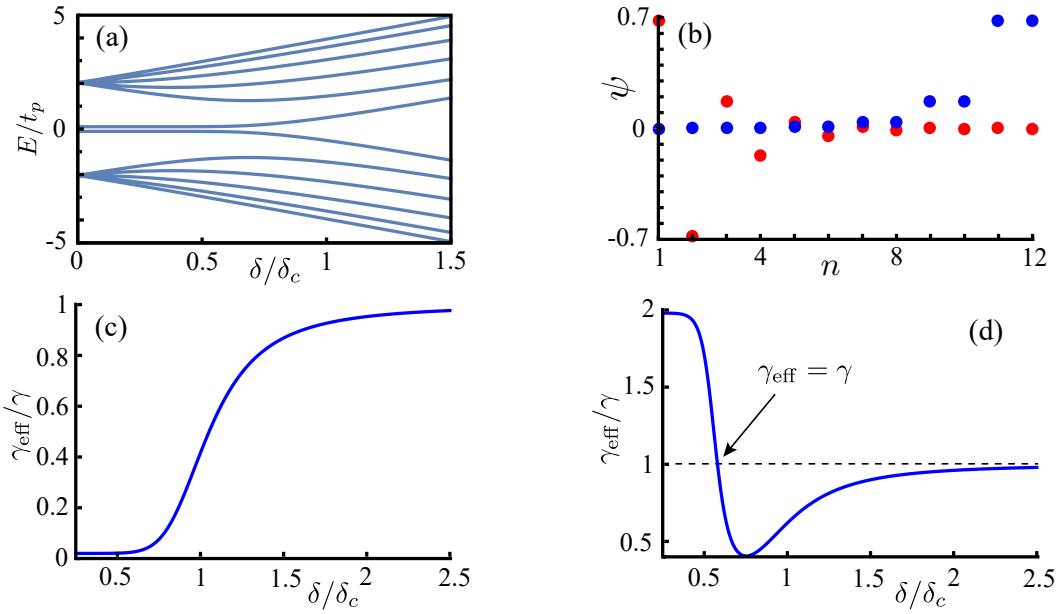

FIG. S8. Effects of interactions between atoms in the same unit cells. (a) The energy degeneracy for edge states is shifted. (b) The hybridized edge state (see Fig. S6(d)) become separated (with $\delta = 0.25\delta_c$). (c) Quantum coherence of the left edge state. (d) Quantum coherence of the right edge state. The parameters we considered here are $t_c = t_p$, $g_{AB} = 0.1\gamma$ and $N = 6$.

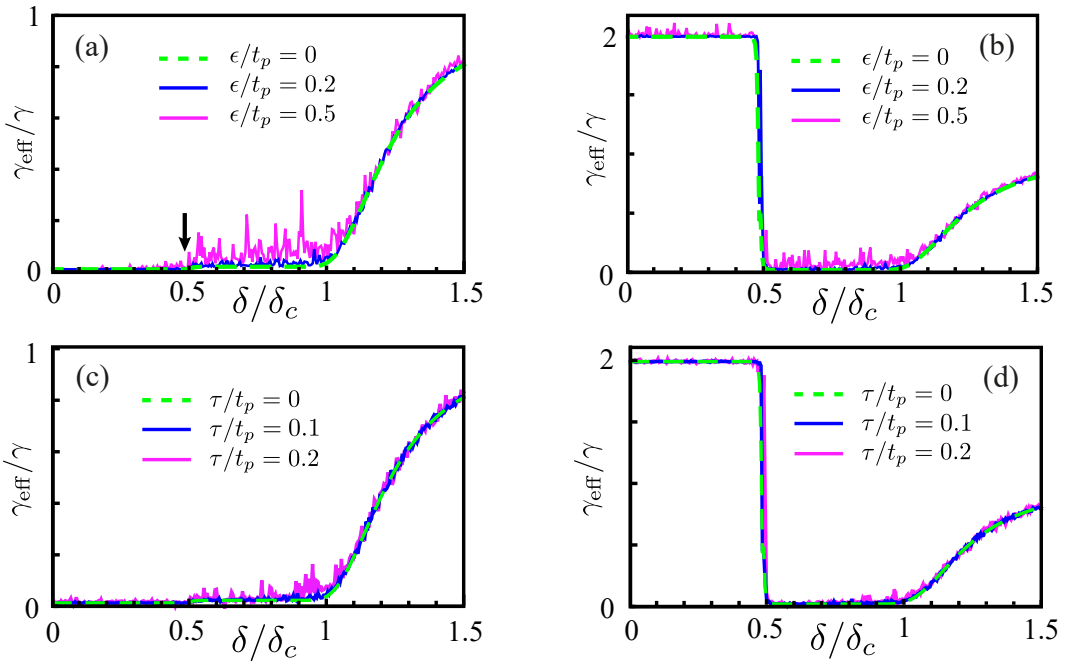

FIG. S9. Disorders of atomic frequencies for (a) subradiant edge state and (b) superradiant edge state. Disorders of atomic interactions for (c) subradiant edge state and (d) superradiant edge state. The parameters are $t_c = t_p, \gamma = 10\kappa, \gamma_{AB} = 0.99\gamma, N = 50$.

are preserved, as shown in Fig. S8(b). Different from Fig. S6(d), the edge states are not hybridized at $\delta = 0.25\delta_c$. The breaking of energy degeneracy for edge states have a nontrivial influence on the topological phase transition. In Figs. S8(c) and S8(d), we show the effective decays for left and right edge states and their transitions to bulk states. Different from the case with chiral symmetry we discussed in the main text, here there is no interaction between edge states during the topological phase transition. And the topological superradiance-subradiance transition, i.e., $\gamma_{\rm eff} = \gamma$ as shown in Fig. S8(d), is produced by the direct edge-bulk transition.

In Figs. S9(a) and S9(b), we study the effect of disorder of atomic frequencies for the subradiant and superradiant edge states, respectively. The atomic frequencies are $\omega_{i\alpha} + \epsilon_{i\alpha}$ $(\alpha = A, B)$, where $\epsilon_{i\alpha}$ are uniformly distributed $\epsilon_{i\alpha} \in [-\epsilon, \epsilon]$. Here, ϵ represents the strength of the disorder. The unhybridized subradiant edge state $(\delta < \delta_m)$ is stable to the noise. However, the hybridized subradiant edge states $(\delta_m < \delta < \delta_c)$ and subradiant bulk states in the non-topological phase $(\delta > \delta_c)$ are more sensitive to the frequency noise. Similar results are found for the noise of atomic interactions, as shown in Figs. S9(c) and S9(d), where the disorder of atomic interactions of strength τ for the subradiant and superradiant edge states are respectively considered. From Figs. S9(a)-S9(d), we find the robustness of quantum coherence to noises for the unhybridized edge states $(\delta < \delta_m)$. And the effect of the noises is enhanced for hybridized edge states $(\delta_m < \delta < \delta_c)$.

[S1] J. H. Béjanin, T. G. McConkey, J. R. Rinehart, C. T. Earnest, C. R. H. McRae, D. Shiri, J. D. Bateman, Y. Rohanizadegan, B. Penava, P. Breul, S. Royak, M. Zapatka, A. G. Fowler and M. Mariantoni, *Three-Dimensional Wiring for Extensible Quantum Computing: The Quantum Socket*, Phys. Rev. Applied **6**, 044010 (2016).

[S2] D. Rosenberg, D. Kim, R. Das, D. Yost, S. Gustavsson, D. Hover, P. Krantz, A. Melville, L. Racz, G. O. Samach, S. J. Weber, F. Yan, J. L. Yoder, A. J. Kerman and W. D. Oliver, *3D integrated superconducting qubits*, npj Quantum Information **3**, 42 (2017).

[S3] A. Dunsworth, R. Barends, Y. Chen, Z. Chen, B. Chiaro, A. Fowler, B. Foxen, E. Jeffrey, J. Kelly, P. V. Klimov, E. Lucero, J. Y. Mutus, M. Neeley, C. Neil, C. Quintana, P. Roushan, D. Sank, A. Vainsencher, J. Wenner, T. C. White, H. Neven, J. M. Martinis and A. Megrant, *A method for building low loss multi-layer wiring for superconducting microwave devices*, Appl. Phys. Lett. **112**, 063502 (2018).

[S4] H. Mukai, K. Sakata, S. J. Devitt, R. Wang, Y. Zhou, Y. Nakajima and J. S. Tsai, *Pseudo-2D superconducting quantum computing circuit for the surface code*, arXiv:1902.07911 (2019).

[S5] A. Gonzalez-Tudela, D. Martin-Cano, E. Moreno, L. Martin-Moreno, C. Tejedor and F. J. Garcia-Vidal, *Entanglement of*

Two Qubits Mediated by One-Dimensional Plasmonic Waveguides, Phys. Rev. Lett. **106**, 020501 (2011).

[S6] M. Mirhosseini, E. Kim, X. Zhang, A. Sipahigil, P. B. Dieterle, A. J. Keller, A. Asenjo-Garcia, D. E. Chang and O. Painter, *Cavity quantum electrodynamics with atom-like mirrors*, Nature **569**, 692 (2019).

[S7] M. König, H. Buhmann, L. W. Molenkamp, T. Hughes, C.-X. Liu, X.-L. Qi and S.-C. Zhang, *The Quantum Spin Hall Effect: Theory and Experiment*, J. Phys. Soc. Jpn. **77**, 031007 (2008).

[S8] X.-J. Liu, X. Liu, C. Wu and J. Sinova, *Quantum anomalous Hall effect with cold atoms trapped in a square lattice*, Phys. Rev. A **81**, 033622 (2010).